Few-boson localization in a continuum with speckle disorder

Pere Mujal,[1,2] Artur Polls,[1,2] Sebastiano Pilati,[3] and Bruno Juliá-Díaz[1,2,4,*]

[1]*Departament de Física Quàntica i Astrofísica, Universitat de Barcelona, Martí i Franquès 1, 08028 Barcelona, Spain*
[2]*Institut de Ciències del Cosmos (ICCUB), Universitat de Barcelona, Martí i Franquès 1, 08028 Barcelona, Spain*
[3]*School of Science and Technology, Physics Division, Università di Camerino, 62032 Camerino (MC), Italy*
[4]*Institut de Ciències Fotòniques, Parc Mediterrani de la Tecnologia, 08860 Barcelona, Spain*

(Received 13 March 2019; published 2 July 2019)

The disorder-induced localization of few bosons interacting via a contact potential is investigated through the analysis of the level-spacing statistics familiar from random matrix theory. The model we consider is defined in a continuum and describes one-dimensional bosonic atoms exposed to the spatially correlated disorder due to an optical speckle field. First, we identify the speckle-field intensity required to observe, in the single-particle case, the Poisson level-spacing statistics, which is characteristic of localized quantum systems, in a computationally and experimentally feasible system size. Then, we analyze the two-body and the three-body systems, exploring a broad interaction range, from the noninteracting limit up to moderately strong interactions. Our main result is that the contact potential does not induce a shift towards the Wigner-Dyson level-spacing statistics, which would indicate the emergence of an ergodic chaotic state, indicating that localization can occur also in interacting few-body systems in a continuum. We also analyze how the ground-state energy evolves as a function of the interaction strength.

DOI: 10.1103/PhysRevA.100.013603

I. INTRODUCTION

Since Anderson's 1958 seminal article [1], it is known that quenched disorder can induce localization of noninteracting quantum particles, determining the absence of transport of any conserved quantity in macroscopic samples. If and when Anderson localization can be stable against interparticle interactions has been an outstanding open question ever since [2–4]. In recent years, this question has been addressed in innumerable theoretical articles, putting forward the theory of so-called many-body localization [5,6]. This phenomenon is expected to occur in isolated one-dimensional systems with disorder. Among other properties, it is characterized by the occurrence of perfect insulating behavior at finite temperature, by the fact that the many-body localized system is unable to act as its own thermal bath, therefore violating the eigenstate thermalization hypothesis, and by the emergence of an extensive number of local integrals of motion. See Refs. [7,8] for recent reviews. While some previous theoretical predictions on many-body localization, based mostly on perturbative calculations, considered continuous-space models [5,6,9,10], most numerically exact simulations considered one-dimensional discrete-lattice models within the tight-binding formalism. In fact, whether many-body localization can occur in a continuum is still a controversial issue. In Ref. [11], it is claimed that many-body localization can occur even in continuous-space systems if the (nondeterministic) disorder is in the impurity limit, but it might be unstable if the correlation length of the disorder is finite. Reference [12], instead, states that many-body localization cannot occur at all in a continuum. On the other hand, the continuous-space simulations of Ref. [13], which considered fermionic atoms in a quasiperiodic (hence, deterministic) potential and were based on time-dependent density-functional theory within the adiabatic approximation, displayed one of the experimental hallmarks of many-body localization; namely, the long-time persistence of an initially imprinted density pattern. This phenomenon has indeed been observed in the cold-atom experiments on many-body localization [14–16]. Also a very recent theoretical study states that many-body localization can be identified in continuous-space (two-dimensional) systems if the appropriate criterion is adopted [17]. Resolving this controversy is essential, given that discrete-lattice models are at most a reasonably good low-energy approximation of experimental systems. In this article, we shed some light on this issue, considering however a few-body setup.

The model we consider is tailored to describe a setup that can be implemented in cold-atom experiments [18,19]. Specifically, it describes bosonic atoms in a one-dimensional continuum, interacting via a repulsive zero-range interaction. The atoms are exposed to the spatially correlated random potential corresponding to the disorder pattern that is generated when an optical speckle field is shone onto the atomic cloud. Due to the higher computational cost of continuous-space models compared with lattice models—for which one could simulate around 10 itinerant particles or, say, 20 or 30 immobile spins—we focus on one-, two-, and three-boson systems. The main goal of our analysis is to verify whether localization is stable against the repulsive contact interparticle interaction, meaning that many-body localization can be observed in a few-body setup. Indeed, many-body localization has recently been experimentally identified for relatively small systems of eight atoms [20]. Previous theoretical studies investigated the interaction effect in continuous-space bosons within the Gross-Pitaevskii theory [21,22].

*Corresponding author: brunojulia@ub.edu

 ©2019 American Physical Society

The theoretical tool we employ to identify localized states is the analysis of the energy-level spacing statistics familiar from quantum chaos and random matrix theories [23,24]. In this framework, one discerns delocalized ergodic states from localized states by identifying the Wigner-Dyson statistical distribution and the Poisson distribution of the level spacings, respectively. This approach has been commonly adopted in studies on single-particle Anderson localization in discrete lattice models [25–28] and, more recently, also in continuous-space (single-particle) models relevant for cold-atoms experiments [29,30]. Chiefly, this approach has been established as one of the most sound criteria to identify many-body localized phases [31] since it allows one to identify the breakdown of ergodicity independently of the specific mechanism causing localization, including, e.g., localization in Fock space. In this context, it has been applied to one-dimensional discrete systems, including spin models [32–35], spinless fermion models [31,36], and recently also to bosonic models [37,38]. Here, we apply it to a continuous-space few-boson model.

The first step we take is to determine, in the single-particle case, the disorder intensity required to observe the statistics of nonergodic systems (i.e., the Poisson level-spacing distribution) for a linear system size that is feasible for our computational approach—and, as a matter of fact, also for cold-atom experiments—in a sufficiently broad low-energy region of the spectrum. Then, we analyze if and how interparticle interactions affect the localization in the two and in the three-particle cases, again analyzing in an energy-resolved manner the level-spacing statistics. This is obtained via large-scale matrix diagonalization calculations of the two-body and three-body Hamiltonians represented in the Fock space corresponding to a suitably chosen basis. A broad range of interaction strengths is considered, ranging from the noninteracting limit, up to strong interaction strengths in the broad vicinity of the strongly interacting limit where the bosons fermionize, meaning that the ground-state energy approaches the value corresponding to a noninteracting fully polarized fermion model. Furthermore, we characterize how the ground-state energy evolves in the crossover between the noninteracting and the strongly interacting limits.

The main result we report is that, for a reasonably broad low-energy portion of the spectrum, the contact interaction does not induce a shift from Poisson to Wigner-Dyson statistics; this statement holds for the full interaction range we consider. This indicates that many-body localization can occur, at low energy, also in continuous-space models, at least in the few-body setup and for the contact-interaction model considered here. The rest of the article is organized as follows: in Sec. II we describe the continuous-space model with speckle disorder and the computational approach we adopt, analyzing in particular the convergence of the energy levels as a function of the basis size. Section III focuses on a single particle in the speckle disorder, analyzing the spatial structure of the eigenstates and the level-spacing statistics. The results for two-boson and three-boson systems are presented in Sec. IV. Our conclusions and the future perspectives are reported in Sec. V.

II. THE HAMILTONIAN

In the general case, the model we consider consists in N identical bosons of mass m in a one-dimensional box of size L, with a random external field $V(x)$ that describes a blue-detuned optical speckle field [39]. The Hamiltonian reads

$$\mathcal{H} = \sum_{i=1}^{N} \left(-\frac{\hbar^2}{2m}\frac{\partial}{\partial x_i} + V(x_i) \right) + \sum_{i<j}^{N} v(|x_i - x_j|). \quad (1)$$

The variables x_i, with the particle label $i = 1, \ldots N$, indicate the particle coordinates. Hard-wall boundary conditions are considered, meaning that the wave functions vanish at the system boundaries. $v(|x_i - x_j|)$ indicates a zero-range two-body interaction potential between particles i and j defined as

$$v(|x_i - x_j|) = g\delta(|x_i - x_j|). \quad (2)$$

The coupling parameter g, which fixes the interaction strength, is related to the one-dimensional scattering length a_0 as $g = -\hbar^2/(ma_0)$. In this work, we consider a repulsive interaction, $g \geqslant 0$. The one-dimensional Hamiltonian (1) accurately describes ultracold gases in one-dimensional waveguides with a tight radial confinement, and the interaction parameter g can be tuned either by varying the radial confining strength and/or tuning the three-dimensional scattering length via Feshbach resonances [40].

The external field $V(x)$ describes the potential experienced by alkali-metal atoms exposed to optical speckle fields. Such fields are generated when coherent light passes through a rough (semitransparent) surface. An efficient numerical algorithm to create speckle fields in computer simulations has been described elsewhere [41–44], and we refer the readers interested in more details about the algorithm to those references.

Fully developed speckle fields in large systems are characterized by an exponential probability distribution of the local intensities V, which reads $P(V) = \exp(-V/V_0)/V_0$ for $V \geqslant 0$, and $P(V) = 0$ for $V < 0$ [39]. Here, $V_0 \geqslant 0$ is the average intensity of the field and coincides with its standard deviation. V_0 is therefore the unique parameter that characterizes the disorder strength.

The two-point spatial correlation function of local intensities of a speckle field depends on the distance d between two given points and reads [42]

$$\Gamma(d) = \frac{\langle V(x+d)V(x)\rangle}{V_0^2} - 1 = [\sin(d\pi/\ell)/(d\pi/\ell)]^2. \quad (3)$$

Here, the brackets $\langle \cdots \rangle$ indicate spatial averages. Notice that in a sufficiently large system, the speckle field is self-averaging, meaning that spatial averages can be replaced by averages of local values over many realizations of the speckle field. The length scale ℓ is related to the inverse of the aperture width of the optical apparatus employed to create the optical speckle field and to focus it onto the atomic cloud. It characterizes the typical distance over which the local intensities lose statistical correlations, or, in other words, the typical size of the speckle grains. In the following, we use this spatial correlation length as unit of lengths, setting $\ell = 1$. This length scale also allows one to define a characteristic energy scale, often referred to as correlation energy, which reads $E_c = \hbar^2/(m\ell^2)$. This quantity will be used in the following as the unit for energies, unless explicitly stated. The interaction parameter g is expressed in units of $\hbar^2/(\ell m)$.

The few-body problem is solved by direct diagonalization of the second-quantized many-body Hamiltonian in a truncated many-body basis [46]. The Hamiltonian (1) is written in second-quantization as the sum of three terms:

$$\hat{H} = \hat{K} + \hat{V} + \hat{v}. \tag{4}$$

Each term can be defined by using the standard creation and annihilation operators $\hat{a}_i^\dagger$ and $\hat{a}_j$ that fulfill the bosonic commutation relations $[\hat{a}_j, \hat{a}_i^\dagger] = \delta_{i,j}$. These operators create or annihilate bosons in the single-particle states, which are taken as the eigenstates of the free particle moving in a one-dimensional box with hard walls. The box size is chosen large enough compared with the spatial correlation length ℓ. The many-body Fock states are defined in terms of the creation operators as

$$|n_1, \ldots, n_M\rangle = \frac{(\hat{a}_1^\dagger)^{n_1} \ldots (\hat{a}_M^\dagger)^{n_M}}{\sqrt{n_1! \cdots n_M!}} |\text{vac}\rangle\,, \tag{5}$$

where $|\text{vac}\rangle$ is the vacuum state and the quantum numbers n_k indicate the number of bosons in the single-particle state k. In all computations, we have $\sum_{k=1}^{M} n_k = N$. In this basis, the kinetic energy $\hat{K}$ has diagonal form,

$$\hat{K} = \sum_k \frac{k^2\pi^2}{2L^2} \hat{a}_k^\dagger \hat{a}_k. \tag{6}$$

The speckle potential reads

$$\hat{V} = \sum_{k,j} V_{k,j} \hat{a}_k^\dagger \hat{a}_j, \tag{7}$$

with

$$V_{k,j} = \int_{-\frac{L}{2}}^{\frac{L}{2}} dx \psi_k^*(x) V(x) \psi_j(x) \tag{8}$$

and

$$\psi_k(x) = \sqrt{\frac{2}{L}} \sin\left[\frac{k\pi}{L}\left(x + \frac{L}{2}\right)\right]. \tag{9}$$

These integrals are determined via numerical quadrature based on the composite five-point Bode's rule, using a sufficiently fine grid so that the residual numerical error due to the discretization is negligible.

The interaction term reads

$$\hat{v} = \frac{g}{2} \sum_{i,j,k,l} v_{ijkl} \hat{a}_i^\dagger \hat{a}_j^\dagger \hat{a}_k \hat{a}_l, \tag{10}$$

with

$$\begin{aligned} v_{ijkl} = \frac{1}{2L}(&-\delta_{i,j+k+l} + \delta_{i,-j+k+l} \\ &+ \delta_{i,j-k+l} - \delta_{i,-j-k+l} + \delta_{i,j+k-l} \\ &- \delta_{i,-j+k-l} - \delta_{i,j-k-l} + \delta_{i,-j-k-l}). \end{aligned} \tag{11}$$

We follow the criterion to truncate the many-body basis discussed in Ref. [47], where its efficiency in terms of computing resources has been highlighted. The many-body basis is built including all states with a kinetic energy equal to or smaller than a given threshold $E_{\max}$. The minimal number of single-particle modes M required to include all such many-body states is retained. The energy threshold $E_{\max}$ represents an algorithmic parameter whose role has to be analyzed. In fact, while the computation is exact in the $E_{\max} \to \infty$ limit, a residual truncation error might occur for finite $E_{\max}$ value. Once the number of bosons and energy threshold are fixed we can build the corresponding many-body Fock basis. Then we construct the Hamiltonian in this Fock basis and diagonalize its low-energy part by means of the ARPACK implementation of the Lanczos method.

TABLE I. Convergence of the ground-state energy for $N = 2$: for a given speckle and in the noninteracting case (forth column) and for $g = 1$ (fifth column); for a harmonic potential and $g = 1$ (sixth column) that should tend to the exact value $E_{GS}^{h.o.} \cong 1.306\,75$ [45]. $E_{\max}$ was used to truncate the many-body Hilbert space by using an energy criterion which required M single-particle states and it corresponds to a many-body Hilbert space dimension D_{MB}. The system size is $L = 100\ell/\sqrt{2}$ and in the cases with a harmonic trap we have set $\sqrt{\hbar/(m\omega)} = \ell$, i.e., $\hbar\omega = E_c$. For the speckle potential $V_0 = 50E_c$.

$E_{\max}$	M	D_{MB}	$E_{GS}(g=0)$	$E_{GS}(g=1)$	$E_{GS}^{h.o.}(g=1)$
20	142	7941	7.0266	7.7813	1.3249
40	201	15889	6.8818	7.5954	1.3191
60	246	23836	6.8328	7.5403	1.3167
100	318	39747	6.8309	7.5338	1.3143
120	348	47697	6.8308	7.5319	1.3136

Table I reports the analysis of the convergence with the energy truncation parameter $E_{\max}$ for a few representative setups. D_{MB} in this table indicates the number of states in the many-body basis set. Specifically, we consider the ground-state energy of two bosons in the noninteracting case ($g = 0$) and with a relatively strong interaction ($g = 1$). Here the disorder strength is set to $V_0 = 50E_c$. One notices that, with the largest basis set, the residual truncation error is much smaller than 0.1%. While the truncation effect becomes somewhat larger at higher energies, we consider in this work an energy range where this effect is negligible. An estimate of the accuracy of our numerical procedure can be obtained by considering the case of two interacting bosons trapped in a harmonic potential, which was exactly solved in Ref. [45]. We choose a harmonic oscillator of length ℓ, which is the typical size of the minima in the speckle potential, within our finite box of size $L = 100\ell/\sqrt{2}$. For an interaction strength $g = 1$ we reproduce the exact results up to the second decimal. This provides a reasonable estimate of the accuracy of our method. Furthermore, we mention here that the results of the analysis of the (ensemble-averaged) level-spacing statistics are less sensitive to the truncation error than the individual energy level of a single realization of the speckle field.

III. LOCALIZATION IN THE SINGLE-PARTICLE CASE

In this article, the occurrence of the localization, i.e., nonergodic behavior, is inspected by analyzing the statistics of the energy-level spacings. As a preliminary step, we start by analyzing the general features of the single-particle modes. Figure 1 displays the single-particle wave functions at low, intermediate, and relatively high energies for a given realization of a speckle field of intensity $V_0 = 50E_c$. The low-energy

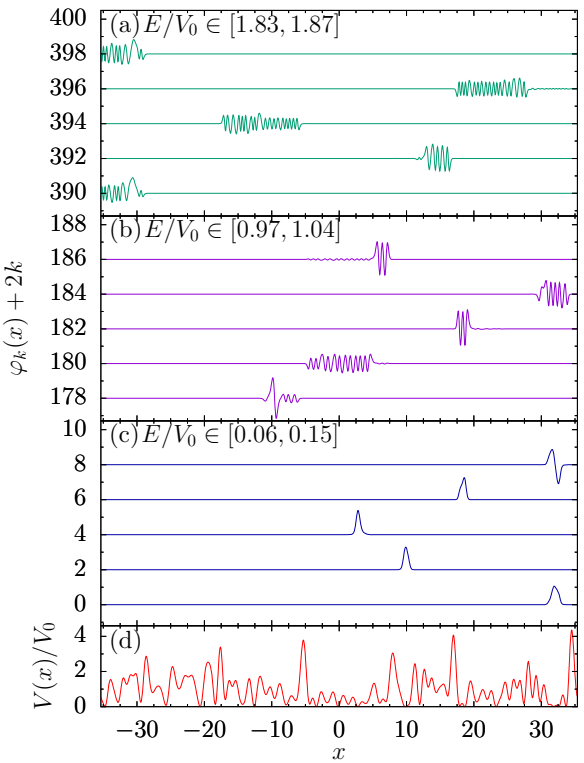

FIG. 1. In panels (a)–(c), we present some eigenfunctions of the speckle potential $V(x)$ from bottom to top, in order of increasing energy in the energy ranges written in the panels. A realization of the speckle potential with $V_0 = 50E_c$ is shown in panel (d). The system size is $L = 100\ell/\sqrt{2}$.

states are located in the Lifshitz tail of the density of states. Here, localization typically occurs in rare regions where the disorder creates a deep well confined by tall barriers. In fact, we observe that the spatial extent where these low-energy states have large amplitude is typically of the order of the disorder correlation length ℓ, meaning that they are indeed localized in a single well of the speckle field. However, this spatial extent rapidly increases as a function of the energy, becoming significantly larger than ℓ. On a qualitative level, this effect can be observed in Fig. 1, noticing that the states at intermediate and at relatively high energies have large amplitude in several wells of the speckle potential. To quantify this spatial extent, we compute the participation ratio, which is defined as $P_k = 1/\int \mathrm{d}x|\varphi_k(x)|^4$. For the low-energy states in the Lifshitz tail, we find, again for $V_0 = 50E_c$, $\langle P_k\rangle \simeq \ell$, indeed corresponding to trapping in a single deep well. Here the brackets $\langle\cdot\rangle$ indicate the average over many realizations of the speckle field. Instead, for states with energies above the average speckle-field intensity, e.g., with energy $E \simeq 2V_0$, the spatial extent is $\langle P_k\rangle \simeq 5\ell$, and it reaches $\langle P_k\rangle \simeq 11\ell$ at $E \simeq 3V_0$. At even higher energies the participation ratio is of the order of the system size (here $L = 100\ell/\sqrt{2}$) and finite-size effects due to the box become dominant. At these energies the single-particle states are weakly affected by the disorder, since in the finite system the speckle field typically develops only moderately high peaks, as opposed to an infinite system where a sufficiently high peak would always occur given that the speckle potential has no upper bound. Clearly, these finite-size effects have to be avoided (see also the discussion on the analysis of the level-spacing statistics reported below). The choice of inspecting that localization occurs in a sufficiently small length scale and in a reasonably broad portion of the energy spectrum, here taken of the order of the average speckle field intensity V_0, is motivated by the aim to address, in the second step, the effects of interparticle interactions. These will indeed induce population of relatively high-energy states even when noninteracting bosons would occupy only deeply localized low-lying modes. In fact, previous lattice calculations predicted that, in one dimension, the localization length of two interacting particles can be significantly larger than the spatial extent of the single-particle states [48]. In three-dimensional (lattice) systems, two-particle interactions could even induce complete delocalization [49]. One should also consider that, in cold-atom experiments, the atomic energy distribution is inevitably broadened by thermal excitations, by interactions, and by the finite spatial spread of the atomic cloud, meaning that localization effects cannot be observed if only very few low-energy states are spatially localized. In this regard, it is worth mentioning that if one aims at experimentally visualizing the exponentially decaying tails of the single-particle states, a feature that characterizes Anderson-localized systems, it is convenient to consider rather weak disorder $V_0 \approx E_c$, since in this regime the spatial extent is much larger than the typical well size. For example, for a speckle-field intensity $V_0 = E_c$ we find $P_k \simeq 20\ell$ at $E = 3V_0$. In this case, in order to avoid finite-size effects in the participation-ratio calculation (and also in the analysis of the level spacing statistics discussed below), a system size larger than $L = 1000\ell/\sqrt{2}$ is required. Such system sizes cannot be addressed with the computational technique we employ for interacting systems, therefore in the following we consider larger disorder strengths where finite-size effects can be more easily suppressed. Anderson localization in strong speckle disorder has been investigated also in Ref. [50].

It is also worth emphasizing that, in an infinite one-dimensional system where the disorder has no upper bound (like the blue-detuned speckle potential), a classical particle is localized at any energy E, just like a quantum particle in the same setup [51]. Indeed, a position in space where $V(x) > E$ always occurs, prohibiting the particle from exploring the whole configuration space, resulting in nonergodic behavior. This scenario is different from the one that occurs in two-dimensional [52] and in three-dimensional systems, where classical particles in a speckle potential are trapped only if their energy is lower than a finite threshold; above this energy threshold a (classical) percolation transition takes place. In particular, in three-dimensional speckle potentials the classical percolation threshold turns out to be a tiny fraction of the average speckle-potential intensity V_0 [44,53]. The mobility edge, i.e., the energy threshold that in three-dimensional quantum systems separates localized states from extended states, is typically much larger than this classical percolation threshold, meaning that in a broad energy range particles are trapped purely by quantum-mechanical effects. In the one-dimensional setup considered here, instead, both quantum and classical particles are localized at any energy in the infinite-size limit, meaning that classical and quantum trapping mechanisms cannot be rigorously separated.

The analysis of the statistical distribution of the spacings between consecutive energy levels allows one to discern localized (i.e., nonergodic) states from delocalized ergodic states. Specifically, localized states are associated with the Poisson distribution of the level spacings, while delocalized states are associated with the Wigner-Dyson distribution typical of random matrices. An efficient procedure to identify these two distributions consists in determining the average over a large ensemble of speckle fields of the following ratio of consecutive level spacings [31]:

$$r_i = \min\left\{\frac{E_{i+1}-E_i}{E_i-E_{i-1}}, \quad \frac{E_i-E_{i-1}}{E_{i+1}-E_i}\right\}. \tag{12}$$

Notice that the ensemble averaging we perform, indicated as $\langle r\rangle$, is energy resolved, meaning that only states within a narrow energy window are considered. This allows us to address possible scenarios where both localized states and delocalized states occur, but in different sectors of the energy spectrum. The Poisson distribution translates to the ensemble average $\langle r\rangle \cong 0.38\,629$, while the Wigner-Dyson distribution translates to $\langle r\rangle \cong 0.530\,70$ [54].

As discussed above, the scaling theory of Anderson localization [51] predicts that, in infinite one-dimensional disordered systems, the localization occurs for any amount of disorder, even if this amount is vanishingly small. However, in finite-size systems the localization length might be comparable to the system size, hindering the observation of the Poisson distribution corresponding to localized systems. This effect is particularly relevant if the disorder is weak or if the energy window under consideration is high, since the localization length is large in these regimes, as previously discussed. It is, therefore, pivotal for our purposes to identify a disorder strength and an energy range where the Poisson statistics can be observed in a system size that is feasible for our computational approach for interacting systems. Figure 2 displays the energy-resolved analysis of the level-spacing statistics for a few representative setups of the optical speckle field. Specifically, Fig. 2(a) shows $\langle r\rangle$ versus E/E_c for a fixed system size and different disorder strengths, while Fig. 2(b) shows data corresponding to different system sizes at a fixed disorder strength. One observes that, at low energy, the $\langle r\rangle$ values precisely agree with the prediction for the Poisson distribution, indicating that the low-energy states are localized on a sufficiently small length scale. However, significant deviations occur at higher energies. We attribute them to the finite-size effect discussed above. In fact, one observes that, for larger system sizes, the Poisson-distribution result extends to higher energies. This finding is consistent with the expectation that, in an infinite system, the whole energy spectrum would be localized. In the following, we consider the system size $L = 100\ell/\sqrt{2}$ and the disorder strength $V_0 = 50E_c$, where the $\langle r\rangle$ values precisely correspond to the statistics of localized systems in a reasonably broad energy range $0 < E \lesssim 100E_c$. Notice that the upper limit is twice as large as the average speckle-field intensity V_0.

It is worth pointing out that the linear system size of typical cold-atom experiments performed with an optical speckle field is comparable to the system size considered here; it ranges from a few tens to around a thousand times the speckle correlation length ℓ. Therefore, this analysis also serves as a guide for experiments on localization phenomena in atomic gases.

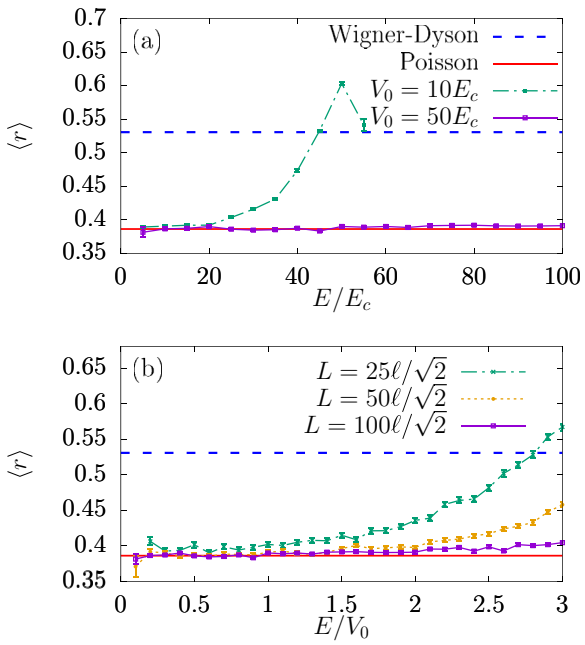

FIG. 2. The value of $\langle r\rangle$ averaged over 2000 different speckle instances is shown. In panel (a) we compare two cases with different speckle intensity, V_0, and in panel (b) with different system sizes. In panel (a) $L = 100\ell/\sqrt{2}$ and in panel (b) $V_0 = 50E_c$. The distribution in energy is computed by using energy windows $\Delta E = 5E_c$. The diagonalization was performed by using a Hilbert space dimensions of 1000.

While the next section is devoted to systems with $N = 2$ or $N = 3$ interacting bosons, we address here the special case of $N > 1$ noninteracting particles. Clearly, the system properties in this case can be traced back to the single-particle problem. However, as we discuss here, special care has to be taken in order to correctly extract the correct level-spacing statistics.

In fact, in certain circumstances, the N-boson energy-level spacings in the noninteracting limit take specific, nonrandom values. For a given realization of the speckle potential, we can distinguish two possible scenarios, depicted in the two panels of Fig. 3, depending on the relative distances of the first and of the second single-particle levels from the single-particle ground-state; they are indicated below as Δ_1 and Δ_2, respectively. For the scenario displayed in Fig. 3(a), where $2\Delta_1 < \Delta_2$, the three lowest-energy eigenstates of the noninteracting N-boson system are

$$|E_0\rangle = |N, 0, \ldots, 0\rangle\,, \quad |E_1\rangle = |N-1, 1, 0, \ldots, 0\rangle\,,$$
$$|E_2\rangle = |N-2, 2, 0, \ldots, 0\rangle\,, \tag{13}$$

and their associated energies are (see Fig. 3)

$$E_0 = NE_{GS}, \quad E_1 = NE_{GS} + \Delta_1, \quad E_2 = NE_{GS} + 2\Delta_1, \tag{14}$$

where E_{GS} is the single-particle ground-state energy. In this situation, the value of r_1 associated with the lowest energy of

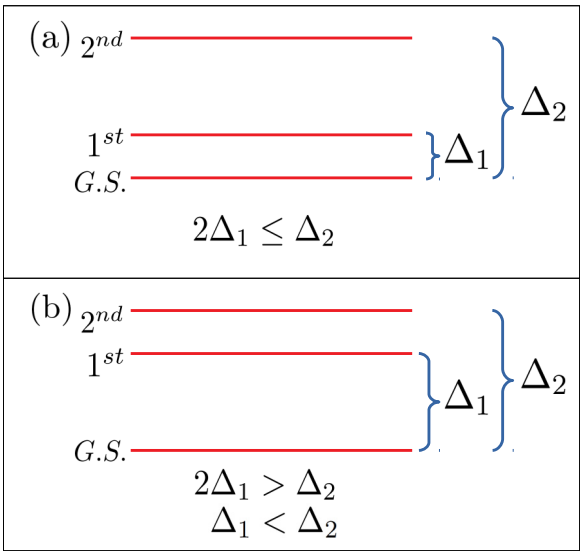

FIG. 3. The lowest single-particle eigenenergies for a given speckle potential determine the lowest energy levels for the noninteracting many-body system. There are two possible situations: (a) a small gap between the single-particle ground state (*G.S.*) and the first-excited state (1^{st}), and (b) a small gap between the first-excited state and the second-excited state (2^{nd}).

the system is

$$r_1 = \frac{E_1 - E_0}{E_2 - E_1} = \frac{\Delta_1}{\Delta_1} = 1. \tag{15}$$

One notices that this does not randomly fluctuate for different speckle-field realizations.

In the second scenario [see Fig. 3(b)], where $2\Delta_1 > \Delta_2$, the three lowest-energy eigenstates of the system are

$$|E_0\rangle = |N, 0, \ldots, 0\rangle\,, \quad |E_1\rangle = |N-1, 1, 0, \ldots, 0\rangle\,,$$
$$|E_2\rangle = |N-1, 0, 1, 0 \ldots, 0\rangle\,, \tag{16}$$

and their associated energies are

$$E_0 = NE_{GS}, \quad E_1 = NE_{GS} + \Delta_1, \quad E_2 = NE_{GS} + \Delta_2. \tag{17}$$

Therefore, we have

$$r_1 = \frac{E_2 - E_1}{E_1 - E_0} = \frac{\Delta_2 - \Delta_1}{\Delta_1}. \tag{18}$$

This is a random variable which depends on the level spacings, and one expects it to follow the Poisson (or eventually the Wigner-Dyson) distribution.

If the data emerging from both scenarios are included in the ensemble average, one obtains, in the low-energy regime, $\langle r\rangle$ values with an upward bias, therefore deviating from the Poisson statistics even in setups where the single-particle modes are localized on a short length scale. This effect, displayed in Fig. 4 for the representative setup with $N = 2, L = 100\ell/\sqrt{2}$, and $V_0 = 50E_c$, should not be associated with a delocalization phenomenon. For this reason, in our calculations with $N > 1$ noninteracting particles we introduce a filter that removes the r_i values which are numerically indistinguishable from $r_i = 1$, i.e., the data corresponding the first scenario described above.

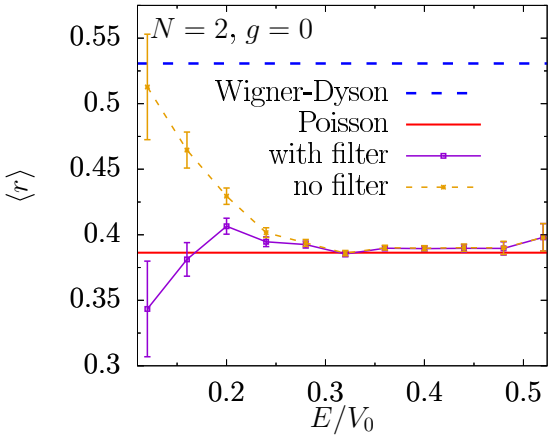

FIG. 4. Mean value of r as a function of E/V_0 distributed in energy computed with and without a randomness filter for the noninteracting two-boson system. The filter removes the values $r_i \geqslant 0.999$.

With this filter, the ensemble-averaged $\langle r\rangle$ values agree with the Poisson-distribution result within statistical uncertainties (see Fig. 4). As expected, the filter has no effect at moderate-to-high energies. It is worth emphasizing that this effect occurs only for noninteracting particles. As soon as $g > 0$, the many-body state is a superposition of many basis states, so the two scenarios described above do not apply and the r_i values randomly fluctuate for different speckle-field realizations.

IV. TWO AND THREE INTERACTING BOSONS

We start the discussion on the interacting few-boson setup with a qualitative analysis of the interaction effect on the ground-state energy. Specifically, we consider $N = 2$ bosons in a speckle field of intensity $V_0 = 50E_c$, in a $L = 100\ell/\sqrt{2}$ box. As discussed in the previous section, in this setup the single-particle modes are spatially localized in a broad energy range $0 < E \lesssim 2V_0$.

In the noninteracting limit, the ground state is the Fock-basis state $|2, 0, \ldots, 0\rangle$, and the corresponding energy equals two times the single-particle ground-state energy. In the first-excited state, one boson is promoted to the first single-particle excited state, obtaining the Fock-basis state $|1, 1, \ldots, 0\rangle$. The energy levels corresponding to the ground state and to the first-excited state of a speckle field instance are displayed in Fig. 5 as a function of the interaction parameter g. One notices that, while the ground-state energy increases with g, the first-excited-state energy is essentially unaltered. This is due to the fact that in the excited state the two bosons are localized in far-apart wells; therefore, the zero-range interaction has an almost negligible effect. In the strongly interacting limit $g \to \infty$, the lowest-energy state is $|1, 1, \ldots, 0\rangle$. This scenario is similar to the Tonks-Girardeau gas, where bosons with infinitely strong zero-range repulsive interaction can be mapped to a system of noninteracting indistinguishable fermions, which occupy different single-particle modes due to the Pauli exclusion principle. Remarkably, the transition between the noninteracting and the strongly interacting regimes is extremely sharp. This effect is due to the long separation between the two lowest-energy minima for this realization of

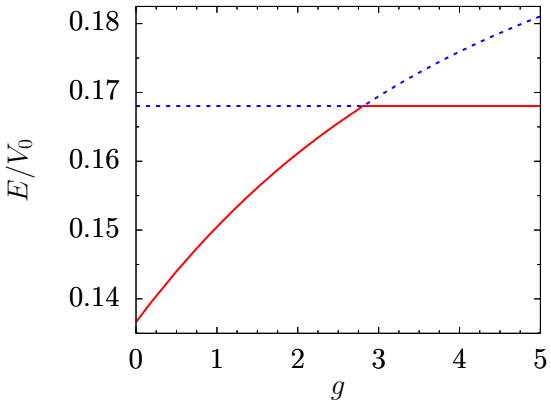

FIG. 5. Energies of the ground state (red solid line) and first-excited state (blue short-dashed line) of the system of $N = 2$ bosons in the speckle potential of Fig. 1(b) as a function of the interaction strength g. This figure is obtained with $M = 636$, which results in a $D_{MB} = 159\,069$ for $E_{\max} = 400$.

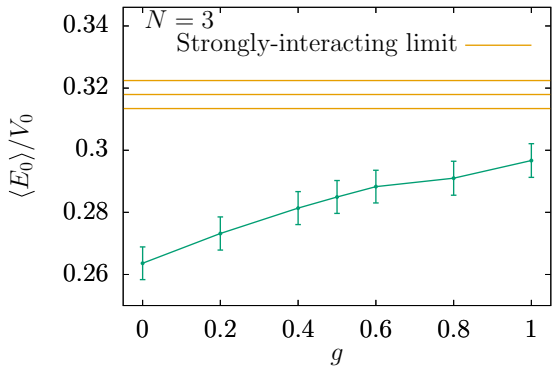

FIG. 7. Mean value of the ground-state energy averaged over $N_s = 250$ different speckle potentials depending on the interaction strength g for the three-boson system. The error bars are computed as the standard deviation, $\sigma_{E_0} = [(\langle E_0^2\rangle - \langle E_0\rangle^2)/N_s]^{1/2}$. The speckle realizations used to produce this plot are the same as those used in Fig. 9.

the speckle potential. For the speckle-field instance analyzed in Fig. 5, this sharp crossover occurs at $g \approx 2.8$. Beyond this pseudocritical point the two-boson system is effectively fermionized, meaning that their ground-state energy essentially coincides with the one of two identical fermions in the same setup. Remarkably, this fermionization occurs at strong but finite values of the interaction parameter g, as opposed to homogeneous systems where bosons fermionize only in the $g \to \infty$ limit, which corresponds to the standard Tonks-Girardeau gas. Note that, in the speckle instances in which the ground and first-excited single-particle states are localized in the same minima, the fermionization would be smoother, in line with, e.g., fermionization in a harmonic potential [55].

For different speckle-field instances, this fermionization transition occurs at different values of the coupling parameter g. Also the energy levels in the noninteracting limit and in the strongly interacting limit, as well as in the crossover region, randomly fluctuate. In Fig. 6, the average over many realizations of the speckle field of the two-boson ground-state energy is plotted as a function of the interaction parameter g. Here, we consider interaction strengths ranging from the noninteracting limit to the moderately large interaction parameter $g = 1$. One notices that this interaction strength is sufficient to shift the ground-state energy away from the noninteracting-limit result, reaching values in fact closer to the strongly interacting limit—where the energy of a noninteracting identical fermions is reached—than to the noninteracting limit. The same scenario occurs for the $N = 3$ boson system, which is analyzed in Fig. 7. In the following, we focus on the interaction regime $0 \leqslant g \leqslant 1$, where any interesting interaction effect would take place. Stronger interactions require extremely large basis-set sizes, so that it is not computationally feasible for us to perform averages of many realization of the speckle field. This regime of intermediate interaction strength $g \approx 1$ is, in fact, the one where one expects to have more pronounced delocalization effects. Indeed, in the strongly interacting limit the system properties are again determined by the single-particle modes. Since the latter are localized for the disorder strength considered here, one expects the many-body system to be localized, too. This type of re-entrant behavior has been observed in the cold-atom experiments on many-body localization [14]. The experimentalists indeed found that, in the strongly interacting limit, the system is many-body localized if the corresponding noninteracting system is localized. The experiment was performed with fermions with two spin states. In this case, in the strongly interacting limit the system properties can be mapped to those of a fully polarized (noninteracting) Fermi gas, in analogy with the Tonks-Girardeau physics in Bose gases.

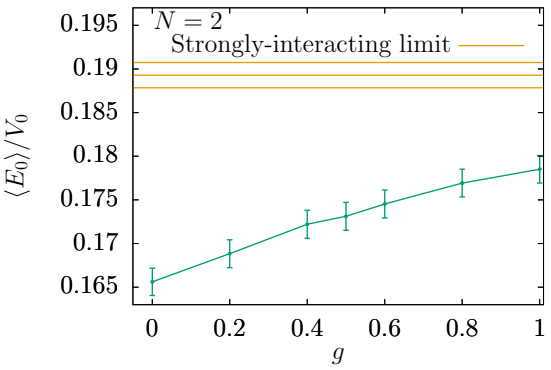

FIG. 6. Mean value of the ground-state energy averaged over $N_s = 985$ different speckle potentials as a function of the interaction strength g for the two-boson system. The error bars are computed as the standard deviation, $\sigma_{E_0} = [(\langle E_0^2\rangle - \langle E_0\rangle^2)/N_s]^{1/2}$. The speckle realizations used to produce this plot are the same as those used in Fig. 8.

The analysis of the level-spacings statistics for the interacting two-boson system is displayed in Fig. 8. Specifically, we plot the disorder-averaged $\langle r\rangle$ values as a function of E/V_0 for different values of the interaction parameter g. The disorder strength V_0 and the linear system size L are those discussed above and in the previous section. We focus on the low-energy regime $E \lesssim V_0$. Accurately computing more energy levels for many speckle-field instances; in particular at high energies where larger basis sets are required, exceeds our computational resources.

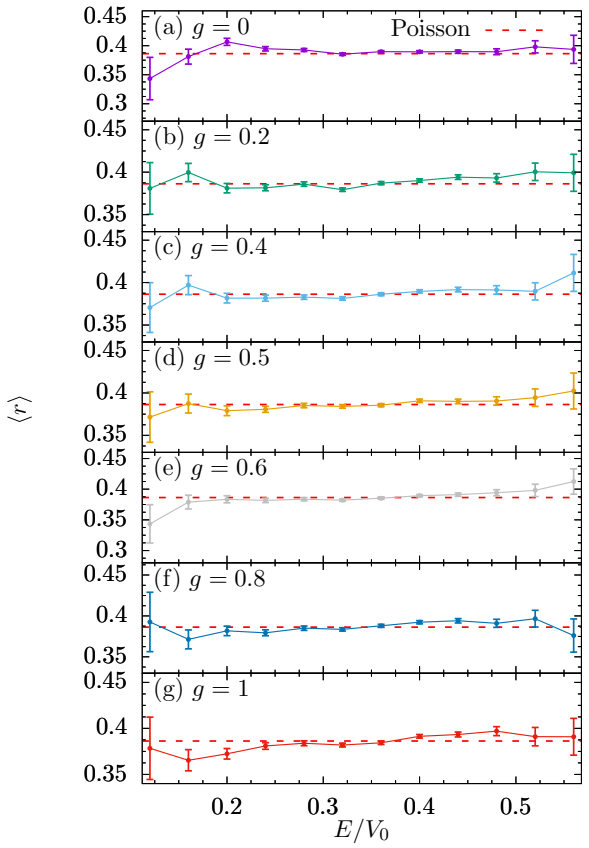

FIG. 8. Distribution in energy of $\langle r \rangle$ for $N = 2$ bosons in a one-dimensional box with a speckle potential. The numerical results with different interaction strengths g of a contact potential are compared with the theoretical value that correspond to a Poisson distribution of the energy gaps.

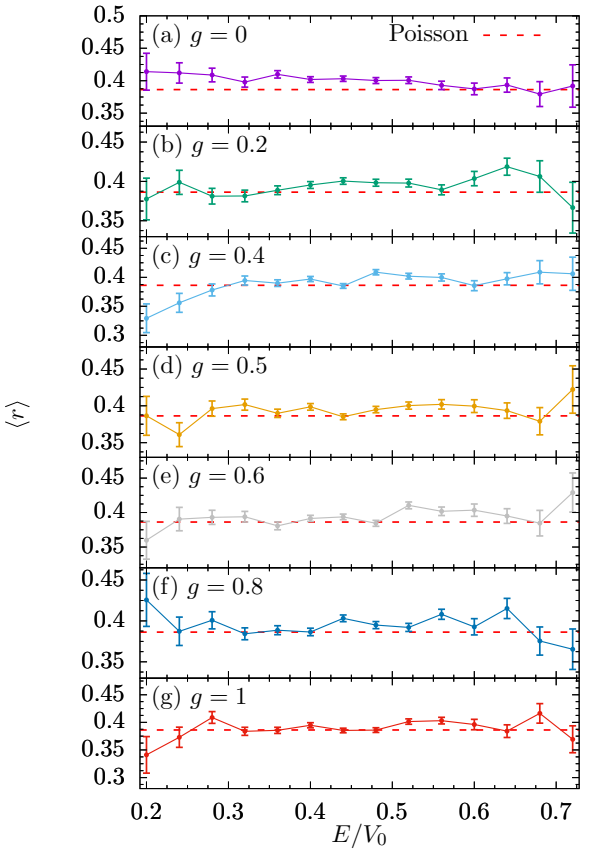

FIG. 9. Distribution in energy of $\langle r \rangle$ for $N = 3$ bosons in a one-dimensional box with a speckle potential for different interaction strengths. The numerical results are compared with the theoretical predictions corresponding to a Poisson distribution of the energy gaps.

For the computations of Fig. 8 the basis sets includes 23 836 states; namely those with a kinetic energy less than or equal to $E_{\max} = 60E_c$; this corresponds to employing $M = 246$ single-particle modes. The disorder ensemble includes 985 realizations of the speckle field.

It is clear that the $\langle r \rangle$ values are always consistent with the prediction corresponding to the Poisson distribution of the level spacings, which is associated with nonergodic systems. The statistical uncertainty is larger in the $E \to 0$ limit due to the low density of states in the low-energy regime, which reduces the available statistics. The agreement with the Poisson distribution implies that, for the range of coupling constant considered here, the zero-range interaction does not induce delocalization of the two-boson system. It is possible that a two-body mobility edge, separating low-energy localized states from high-energy extended states, would occur at higher energies. However, addressing the higher energies requires larger computational resources and is beyond the scope of the present article.

The results for the $N = 3$ boson systems are shown in Fig. 9. Here, the basis-set size is 117 977, corresponding to the Fock-basis states with a kinetic energy less than or equal to $E_{\max} = 12E_c$, in turn implying the use of $M = 110$ single-particle modes. The disorder-ensemble includes 250 realizations of the speckle field. We observe that, also in the three-boson system, localization is, in the low-energy regime and for the coupling parameters considered here, stable against the effect of zero-range interactions.

V. SUMMARY AND CONCLUSIONS

We have performed a computational investigation to establish if and how zero-range repulsive interactions can induce ergodic behavior in an otherwise localized system. While previous computational investigations on this critical issue addressed discrete-lattice models, we focused here on a model defined in continuous space. Specifically, we considered a one-dimensional model which describes ultracold atoms exposed to random optical speckle patterns, taking into account the structure of the spatial correlations of the disorder field. This is the setup that was implemented in early cold-atom experiments on Anderson localization.

The computational procedure we employed is based on exact-diagonalization calculations, combined with the statistical analysis of the levels-spacings statistics familiar from random matrix theory. This is, in fact, one of the most sound criterion commonly employed to identify localized (i.e., nonergodic) phases in noninteracting as well as in interacting disordered systems, where it allows us to identify many-body localized phases.

As a preliminary step, we identified the speckle-field intensity required to observe the (Poisson) statistics of localized systems in a finite linear system size that is feasible for our computational approach and for cold-atom experiments. Our main finding is that, if two or three interacting bosons move in such a speckle field, the localization is stable against zero-range interparticle interactions in a broad range of interactions strengths, ranging from the noninteracting limit, up to moderately strong interactions halfway to the strongly interacting limit. Addressing even stronger interactions is beyond the scope of this article since, on the one hand, it would require larger computational resources and, on the other hand, delocalization effects due to interactions are not expected in this regime since in the strongly interacting limit the system properties are determined by the single-particle modes. Our results are limited to a low-energy regime, of the order of the speckle-field intensity $E \lesssim V_0$, where the accuracy of the diagonalization results is under control. It is possible that, at higher energies, two-body or three-body mobility edges would occur. We leave this question to future investigations.

Previous studies on the possible occurrence of many-body localization in continuous-space systems have provided contradictory results. The findings reported here establish that, in a few-body system, localization can be stable against zero-range interactions in a continuous-space models relevant for cold-atom experiments.

We conclude by formulating two additional interesting questions that naturally emerge from the previous discussion: (i) would finite-range or long-range interactions induce delocalization in an otherwise localized system? (ii) Would a localization-delocalization transition take place if more particles were included? We leave these two question to future investigations.

ACKNOWLEDGMENTS

We acknowledge financial support from the Spanish Ministerio de Economia y Competitividad Grant No FIS2017-87534-P. P.M. is supported by a FI PhD grant from Generalitat de Catalunya. S.P. acknowledges financial support from the FAR2018 project of the University of Camerino, and the CINECA award under the ISCRA initiative, for the availability of high-performance computing resources and support. S.P. also acknowledges travel support from ICCUB.

[1] P. W. Anderson, Phys. Rev. **109**, 1492 (1958).
[2] L. Fleishman and P. W. Anderson, Phys. Rev. B **21**, 2366 (1980).
[3] M. P. A. Fisher, P. B. Weichman, G. Grinstein, and D. S. Fisher, Phys. Rev. B **40**, 546 (1989).
[4] B. L. Altshuler, Yu. Gefen, A. Kamenev, and L. S. Levitov, Phys. Rev. Lett. **78**, 2803 (1997).
[5] I. V. Gornyi, A. D. Mirlin, and D. G. Polyakov, Phys. Rev. Lett. **95**, 206603 (2005).
[6] D. M. Basko, I. L. Aleiner, and B. L. Altshuler, Ann. Phys. (NY) **321**, 1126 (2006).
[7] R. Nandkishore and D. A. Huse, Annu. Rev. Condens. Matter Phys. **6**, 15 (2015).
[8] F. Alet and N. Laflorencie, C. R. Phys. **19**, 498 (2018).
[9] I. L. Aleiner, B. L. Altshuler, and G. V. Shlyapnikov, Nat. Phys. **6**, 900 (2010).
[10] G. Bertoli, V. P. Michal, B. L. Altshuler, and G. V. Shlyapnikov, Phys. Rev. Lett. **121**, 030403 (2018).
[11] R. Nandkishore, Phys. Rev. B **90**, 184204 (2014).
[12] I. V. Gornyi, A. D. Mirlin, M. Müller, and D. G. Polyakov, Ann. Phys. (Berlin, Ger.) **529**, 1600365 (2017).
[13] F. Ancilotto, D. Rossini, and S. Pilati, Phys. Rev. B **97**, 155107 (2018).
[14] M. Schreiber, S. S. Hodgman, P. Bordia, H. P. Lüschen, M. H. Fischer, R. Vosk, E. Altman, U. Schneider, and I. Bloch, Science **349**, 842 (2015).
[15] H. P. Lüschen, P. Bordia, S. Scherg, F. Alet, E. Altman, U. Schneider, and I. Bloch, Phys. Rev. Lett. **119**, 260401 (2017).
[16] J.-Y. Choi, S. Hild, J. Zeiher, P. Schauss, A. Rubio-Abadal, T. Yefsah, V. Khemani, D. A. Huse, I. Bloch, and C. Gross, Science **352**, 1547 (2016).
[17] G. Bertoli, B. L. Altshuler, and G. V. Shlyapnikov, arXiv:1903.07352.
[18] G. Roati, C. D'Errico, L. Fallani, M. Fattori, C. Fort, M. Zaccanti, G. Modugno, M. Modugno, and M. Inguscio, Nature (London) **453**, 895 (2008).
[19] J. Billy, V. Josse, Z. Zuo, A. Bernard, B. Hambrecht, P. Lugan, David Clément, L. Sanchez-Palencia, P. Bouyer, and A. Aspect, Nature (London) **453**, 891 (2008).
[20] A. Lukin, M. Rispoli, R. Schittko, M. E. Tai, A. M. Kaufman, S. Choi, V. Khemani, J. Léonard, and M. Greiner, Science **364**, 256 (2019).
[21] P. Lugan, D. Clément, P. Bouyer, A. Aspect, M. Lewenstein, and L. Sanchez-Palencia, Phys. Rev. Lett. **98**, 170403 (2007).
[22] M. Piraud, P. Lugan, P. Bouyer, A. Aspect, and L. Sanchez-Palencia, Phys. Rev. A **83**, 031603(R) (2011).
[23] M. L. Mehta, *Random Matrices* (Academic Press, Amsterdam, 2004).
[24] F. Haake, *Quantum Signatures of Chaos* (Springer, Berlin, 2010).
[25] B. I. Shklovskii, B. Shapiro, B. R. Sears, P. Lambrianides, and H. B. Shore, Phys. Rev. B **47**, 11487 (1993).
[26] E. Hofstetter and M. Schreiber, Phys. Rev. B **49**, 14726 (1994).
[27] F. Milde, R. A. Römer, and M. Schreiber, Phys. Rev. B **61**, 6028 (2000).
[28] L. Schweitzer and H. Potempa, J. Phys.: Condens. Matter **10**, L431 (1998).
[29] E. Fratini and S. Pilati, Phys. Rev. A **91**, 061601(R) (2015).
[30] E. Fratini and S. Pilati, Phys. Rev. A **92**, 063621 (2015).
[31] V. Oganesyan and D. A. Huse, Phys. Rev. B **75**, 155111 (2007).
[32] A. Pal and D. A. Huse, Phys. Rev. B **82**, 174411 (2010).
[33] E. Cuevas, M. Feigel'man, L. Ioffe, and M. Mezard, Nat. Commun. **3**, 1128 (2012).
[34] D. J. Luitz, N. Laflorencie, and F. Alet, Phys. Rev. B **91**, 081103(R) (2015).
[35] C. R. Laumann, A. Pal, and A. Scardicchio, Phys. Rev. Lett. **113**, 200405 (2014).
[36] P. Naldesi, E. Ercolessi, and T. Roscilde, SciPost Phys. **1**, 010 (2016).
[37] P. Sierant, D. Delande, and J. Zakrzewski, Phys. Rev. A **95**, 021601(R) (2017).
[38] P. Sierant and J. Zakrzewski, New J. Phys. **20**, 043032 (2018).

[39] J. Goodman, *Speckle Phenomena in Optics: Theory and Applications* (Roberts, Englewood, 2007).
[40] M. Olshanii, Phys. Rev. Lett. **81**, 938 (1998).
[41] J. M. Huntley, Appl. Opt. **28**, 4316 (1989).
[42] M. Modugno, Phys. Rev. A **73**, 013606 (2006).
[43] T. Okamoto and S. Fujita, J. Opt. Soc. Am. A **25**, 3030 (2008).
[44] S. Pilati, S. Giorgini, M. Modugno, and N. Prokof'ev, New J. Phys. **12**, 073003 (2010).
[45] T. Busch, B.-G. Englert, K. Rzazewski, and M. Wilkens, Found. Phys. **28**, 549 (1998).
[46] D. Raventós, T. Graß, M. Lewenstein, and B. Juliá-Díaz, J. Phys. B: At. Mol. Opt. Phys. **50**, 113001 (2017).
[47] M. Płodzień, D. Wiater, A. Chrostowski, and T. Sowiński, arXiv:1803.08387.
[48] D. L. Shepelyansky, Phys. Rev. Lett. **73**, 2607 (1994).
[49] F. Stellin and G. Orso, arXiv:1903.06214.
[50] M. Hilke and E. Hichem, Ann. Phys. (Berlin, Ger.) **529**, 1600347 (2017).
[51] E. Abrahams, P. W. Anderson, D. C. Licciardello, and T. V. Ramakrishnan, Phys. Rev. Lett. **42**, 673 (1979).
[52] A. Weinrib, Phys. Rev. B **26**, 1352 (1982).
[53] F. Jendrzejewski, A. Bernard, K. Müller, P. Cheinet, V. Josse, M. Piraud, L. Pezzé, L. Sanchez-Palencia, A. Aspect, and P. Bouyer, Nat. Phys. **8**, 398 (2012).
[54] Y. Y. Atas, E. Bogomolny, O. Giraud, and G. Roux, Phys. Rev. Lett. **110**, 084101 (2013).
[55] F. Deuretzbacher, K. Bongs, K. Sengstock, and D. Pfannkuche, Phys. Rev. A **75**, 013614 (2007).